Published in final edited form as:
Biomech Model Mechanobiol. 2014 August ; 13(4): 801–812. doi:10.1007/s10237-013-0535-7.

Dynamic permeability of the lacunar–canalicular system in human cortical bone

M. Benalla, **P. E. Palacio-Mancheno**, **S. P. Fritton**, **L. Cardoso**, and **S. C. Cowin**
Department of Biomedical Engineering, The City College of New York, Steinman Hall, 160 Convent, New York, NY, USA

L. Cardoso: cardoso@engr.ccny.cuny.edu; S. C. Cowin: sccowin@gmail.com

Abstract

A new method for the experimental determination of the permeability of a small sample of a fluid-saturated hierarchically structured porous material is described and applied to the determination of the lacunar–canalicular permeability (K_{LC}) in bone. The interest in the permeability of the lacunar–canalicular pore system (LCS) is due to the fact that the LCS is considered to be the site of bone mechanotransduction due to the loading-driven fluid flow over cellular structures. The permeability of this space has been estimated to be anywhere from 10^{-17} to 10^{-25} m^2. However, the vascular pore system and LCS are intertwined, rendering the permeability of the much smaller-dimensioned LCS challenging to measure. In this study, we report a combined experimental and analytical approach that allowed the accurate determination of the K_{LC} to be on the order of 10^{-22} m^2 for human osteonal bone. It was found that the K_{LC} has a linear dependence on loading frequency, decreasing at a rate of 2×10^{-24} m^2/Hz from 1 to 100 Hz, and using the proposed model, the porosity alone was able to explain 86 % of the K_{LC} variability.

Keywords

Bioengineering; Biomechanics; Human cortical bone; Interstitial fluid flow; Dynamic bone permeability

1 Introduction

Almost two decades ago, it was first proposed that the amplification of the mineralized tissue strain levels needed for osteocyte mechanosensation occurs when interstitial fluid flow is enhanced by the time-varying mechanical loads applied to bone (Weinbaum et al. 1994; You et al. 2001). Bone interstitial fluid flows through different discrete levels of porosity that coexist in cortical bone, which are nested hierarchically one inside another as a set of Russian dolls in microcirculatory pathways (Cowin et al. 2009). The largest pore size (~25 μm radius) is associated with the vascular porosity, which consists of the volume of all

Correspondence to: S. C. Cowin, sccowin@gmail.com.

Present address: M. Benalla, Department of Mechanical Engineering, Georgia Southern University, P.O. Box 8046, Statesboro, GA 30460, USA

Conflict of interest All authors state that they have no conflicts of interest.

the tunnels in bone that contains blood vessels, nerves, and bone interstitial fluid and includes all the osteonal canals (primary and secondary) as well as transverse (Volkmann) canals (Malachanne et al. 2008; Li et al. 1987; Wen et al. 2010). The lacunar–canalicular porosity contains the osteocytes and bone fluid and consists of the volumes of all the osteocyte lacunae (~3–10 μm radius) and the canaliculi channels (~0.15–0.55 μm diameter) (Marotti 1990). The space between the osteocyte and the lacunar–canalicular wall is filled by the osteocyte's glycocalyx and interstitial fluid. The smallest pore size in bone (<1 nm) is found in the collagen–apatite porosity, where most of the water is bound to ionic crystals in bone (Neuman et al. 1953; Wehrli and Fernandez-Seara 2005). A detailed review of interstitial fluid flow and mechanotransduction in bone was recently presented by Fritton and Weinbaum (2009).

The permeability (inverse of flow resistivity) of the lacunar–canalicular system (LCS) is a critical determinant of interstitial bone fluid flow, which is considered as the main mechanism to stimulate osteocyte cell processes in the LCS and initiate bone mechanotransduction. Accordingly, changes in the lacunar–canalicular permeability may play a key role in bone mechanotransduction as well as in the ability of bone to adapt its local tissue mass and architecture to its mechanical environment (Weinbaum et al. 1994; Cowin et al. 2009; Fritton and Weinbaum 2009). The permeability of the vascular system (K_V) has been estimated from the vascular pore architecture (Johnson 1984; Dillaman 1984; Zhang et al. 1998; Swan et al. 2003) and has been experimentally measured using a traditional technique based on Darcy's law (Rouhana et al. 1981; Li et al. 1987; Wen et al. 2010). This technique consists of measuring the volume of fluid flow per unit area and per unit time across a porous layer, which is then divided by the pore pressure gradient across the layer. Reported estimates and measurements of permeability associated with the vascular porosity span several orders of magnitude (10^{-11} to 10^{-17} m^2). Unfortunately, Darcy permeability measurements are experimentally unfeasible for assessing the LCS permeability (K_{LC}). The LCS permeability has been derived from theoretical analysis of the fluid flow in the pore architecture of the LCS and from combined experimental–numerical–analytical approaches using bone tissue from animal models. Theoretical estimates of K_{LC} reported in the literature span several orders of magnitude, ranging from 10^{-17} to 10^{-20} m^2, while experimental studies have reported a different range of LCS permeability, from 10^{-22} to $10^{-25}m^2$. This wide range of values and the difference between theoretical and measured LCS permeability suggests that the permeability of the lacunar–canalicular system has not been determined with sufficient accuracy to date.

Measurements of the intrinsic lacunar–canalicular permeability of human cortical bone are scarce, and the effect of loading frequency on the dynamic permeability of the lacunar–canalicular system is practically unknown (Cardoso et al. 2013). In order to eliminate the influence of the vascular permeability in experimental measurements of the lacunar–canalicular permeability, Gailani and Cowin (2008) proposed to perform the permeability measurement in samples containing the lacunar–canalicular porosity only, such as a single osteon. An analytical solution of a saturated compressible poroelastic annular cylinder under an unconfined stress relaxation test was developed, and predictions from this model were compared to experimental stress relaxation measurements made on isolated osteons in vitro,

i.e., considering zero blood pressure (Gailani et al. 2009; Gailani and Cowin 2008, 2011). Recently, a frequency-dependent analytical model of a fluid-saturated porous annular cylinder subjected to an axial cyclic strain loading was developed by Benalla et al. (2012). Formulas for the loss tangent, $\tan[\delta(\bar{\omega})]$, representing the frequency-dependent time-delay between the sinusoidal stress and strain in the LCS, were obtained as a function of the lacunar–canalicular permeability in the radial direction and loading frequency. In the present study, this frequency-dependent analytical model (Benalla et al. 2012) and measurements of loss tangent on isolated human osteons under harmonic loading are used (1) to determine the intrinsic lacunar–canalicular permeability in the radial direction of fresh osteonal samples, (2) to assess the effect of time post-isolation of osteons on lacunar–canalicular permeability measurements, (3) to evaluate the effect of loading frequency on the dynamic permeability of the lacunar–canalicular system, and (4) to investigate the relationship between porosity and permeability in the LCS.

2 Materials and methods

2.1 Formulation of the loss tangent with respect to frequency

The analytical model developed in Benalla et al. (2012) considers a transverse segment of an isolated osteon whose annular region (LCS) between the Haversian canal and cement line is subjected to an axial cyclic loading between two smooth, parallel, and impermeable plates. The contact between the specimen and the plates is assumed to be frictionless, and the applied load is considered to be uniformly distributed on the loaded surface. For boundary conditions, free flow is assumed between the LCS and the vascular pore system (VS) and zero flow is considered at the cement line boundary. The axial loading in the form of an applied strain is

$$\varepsilon(t)=\varepsilon_o e^{i\omega t}, \quad (1)$$

where ε_o and ω are the amplitude and frequency, respectively. Under the same assumptions (Cowin et al. 2009) but for zero blood pressure, the governing equation of the pore pressure that leads to a permeability and frequency-dependent relationship between stress and strain was found to be (Benalla et al. 2012)

$$\sigma^*(t)=C^*(\bar{\omega})\varepsilon(t), \quad (2)$$

where $\bar{\omega}$ is the dimensionless frequency (Table 2 in Benalla et al. 2012) and the complex-valued modulus, $C^*(\bar{\omega})$, is given by

$$C^*(\bar{\omega})=C^d_{zz}+\frac{c_1-c_2K_{rr}}{c_3K_{rr}+c_4}-\frac{c_5}{K_{rr}}, \quad C^*(\bar{\omega})=C_o e^{-i\delta(\bar{\omega})} \quad \text{and} \quad C_o=\frac{\sigma_o}{\varepsilon_o}. \quad (3)$$

The magnitude and phase of $C^*(\bar{\omega})$ depend on the c_i (i = 1 – 5), C^d_{zz} is the axial elastic normal stress constant, Krr is the lacunar–canalicular permeability in the radial direction (also simply referred to as K_{LC}), and σ_o is the magnitude of the average resultant stress in

the osteon, while $\delta(\bar{\omega})$ is the phase angle between the applied strain and the resultant stress. Based on Euler's formula, the dynamic modulus $C^*(\bar{\omega})$ can be written as

$$C^*(\bar{\omega}) = C_o e^{i\,\delta(\bar{\omega})} = C_o \cos[\delta(\bar{\omega})] + i C_o \sin[\delta(\bar{\omega})] = C'(\bar{\omega}) + i C''(\bar{\omega}), \quad (4)$$

where $C'(\bar{\omega})$ is known as the storage modulus and $C''(\bar{\omega})$ as the loss modulus of the cyclically loaded osteon. From Eq. (4), the expression of the loss tangent is

$$\tan[\delta(\bar{\omega})] = \frac{C''(\bar{\omega})}{C'(\bar{\omega})} = \frac{\sin[\delta(\bar{\omega})]}{\cos[\delta(\bar{\omega})]}. \quad (5)$$

Formulas for the storage modulus, loss modulus and $\tan[\delta(\bar{\omega})]$ are presented in equations (29) and (30), respectively, in Benalla et al. (2012).

2.2 Formulation of the K_{LC} with respect to loss tangent and frequency

In order to express the K_{LC} with respect to $\tan[\delta(\bar{\omega})]$ and frequency, Eq. (3) is reformulated as

$$K_{rr}^2 (C_{zz}^d c_3 - c_2 - C^* c_3) + K_{rr} (C_{zz}^d c_4 - C^* c_4 - c_5 c_3) - c_5 c_4 = 0. \quad (6)$$

Separating Eq. (6) into real and imaginary parts gives

$$\beta_1 K_{rr}^2\ (\omega) + \beta_2 K_{rr}\ (\omega) + \beta_3 + i\ \left(\alpha_1 K_{rr}^2\ (\omega) + \alpha_2 K_{rr}\ (\omega) + \alpha_3\right) = 0, \quad (7)$$

where β_n and $\alpha_n (n = 1, 3)$ are the coefficients of the two quadratic expressions in Eq. (7). Solutions of the quadratic expressions provide values of the K_{LC} with respect to specified frequency values: $C^*(\bar{\omega})$ is a component of the coefficients in the quadratic Eq. (6). Using Eqs. (4) and (5), $C^*(\bar{\omega})$ is expressed with respect to $\tan[\delta(\bar{\omega})]$ as

$$C^*(\bar{\omega}) = \frac{C_o}{\sqrt{\tan^2[\delta(\bar{\omega})] + 1}} 1 + i \tan[\delta(\bar{\omega})]. \quad (8)$$

Equation (8) permits the computation of complex modulus $C^*(\bar{\omega})$ based on the experimental data of $\tan[\delta(\bar{\omega})]$ at different loading frequencies.

2.3 Sample preparation

Approximately one hundred osteons were extracted from the mid-diaphysis of fresh frozen femurs from three human female donors provided by the National Disease Resource Center. The ages of the donors were 53, 62, and 75 years old, and their medical history excluded any metabolic bone diseases or skeletal cancer. Femurs were kept at −80°C prior to cutting a 10-mm-length segment from the mid-diaphysis. Cortical segments were thawed, cleaned of soft

tissue and bone marrow. Then 0.5-mm-thick cross-sections were machined from each segment using a low-speed diamond saw to obtain smooth and parallel surfaces. Each 0.5-mm-thick section was placed on the stage of an inverted biological microscope equipped with a small drilling machine and a diamond drill bit that was aligned with the center of the microscope field of view. An osteon with a circular or near circular shape was identified using the microscope and carefully isolated.

2.4 Micromechanical loading

A small uniaxial cyclic loading apparatus was developed to measure the stress produced in a single osteon undergoing harmonic strain. The experimental device works under displacement control using a digital controller connected in a closed loop to a piezoelectric linear actuator (P-841.10, Physik Instrumente, Auburn, MA). The linear actuator has a maximal push/pull force of 5 N and a minimal displacement increment of 3 nm. The piezoelectric actuator is vertically aligned to a 10 g load cell (Transducer Techniques, Temecula, CA). The osteon is placed over a stainless steel platen at the top of the load cell, immersed in PBS solution, preloaded, and cyclically strained with the piezoelectric actuator under frequencies ranging from 1 to 100 Hz. The cyclic strains applied by the piezoelectric actuator as well as the resultant stresses acquired from the load cell were collected with Lab-View and analyzed in MATLAB to determine the phase angle δ

Experiment 1. Effect of osteon's storage time on the loss tangent measurements—The change in mechanical properties of post-mortem fresh frozen tissue due to the time elapsed after being thawed for experimental testing was investigated. For this purpose, two subsets of osteon specimens were cyclically loaded with a magnitude of 1,000 $\mu\varepsilon$ and 1 Hz frequency. The first set (9 osteons) was loaded five times every 60 min, hereafter designated as the *hourly* group. The second set (9 osteons) was loaded every 24 h for 5 days, and is henceforth named the *daily* group. Samples in the *daily* group were stored in PBS at −20°C and thawed before testing every day. Data from these tests determined the maximal time between the isolation and mechanical loading of the osteons in which changes in properties of the tissue are small, defining a time window to perform the experimental tests.

Experiment 2. Measurement of osteon's loss tangent and K_{LC} at different frequencies—A second experiment was performed to determine tan $[\bar{\delta}(\omega)]$ and K_{rr} as a function of frequency in a larger set of samples. At twelve different frequencies (1, 2, 3, 5, 8, 10, 15, 20, 30, 50, 70, 100 Hz), cyclic strain was applied to all osteons, and the related tan$[\bar{\delta}(\omega)]$ was measured individually. The loss tangent was measured based on the slope between the applied strain and the resultant stress that determines the phase angle. Then, the K_{LC} of each osteon was obtained based on curve fitting loss tangent experimental data to the analytical model over the range of loading frequencies. Prior to curve fitting of data into the model, the lacunar–canalicular porosity (φ_{LC}), Haversian canal radius, cement line radius, and mineralized tissue elastic modulus were obtained for each osteon based on high-resolution μCT images, light microscope images of the osteons, and a structural model of the LCS morphology, as described in the following sections.

2.5 μCT scanning

After micromechanical testing, osteons were scanned using a high-resolution μCT system (1172 SkyScan, Belgium). X-ray projections were generated from the sample every 0.3°, obtaining 680 consecutive views with 2.1-μm resolution (Nrecon, V.1.6.9, Skyscan, Belgium). Images were density calibrated in Hounsfield Units (HU) and mineral density, ρ_{HA}, using a calibration scan containing air, water, and two density phantoms (0.25 and 0.75 g/cm^3 of hydroxyapatite). Cortical bone was segmented using a global thresholding procedure to exclude the volumes corresponding to the lacunae and the Haversian canal. Segmented cortical bone images were used to calculate the average tissue mineral density (TMD) in the tissue matrix of each osteon. In addition to the TMD, the total number of lacunae, the volume of the lacunae, and the dimensions of each osteon were determined. Also, μCT images were used to determine the alignment of the Haversian canal at the center of the sample and the absence of cracks or inhomogeneities (i.e., resorption areas) that might increase the sample's permeability. Osteons that did not meet these requirements were discarded. A total of 18 osteons were retained for *experiment 1* and 60 osteons for *experiment 2*.

2.6 Measurement of lacunar–canalicular porosity (ϕ_{LC})

The lacunar–canalicular porosity was estimated for each tested osteon as the sum of the lacunar porosity, ϕ_{Lac} (%), and the canalicular porosity, ϕ_{Can} (%). The lacunar porosity was assessed by automated 3D counting of closed porosities within the osteon specimen (CTAn, V.1.13, SkyScan, Belgium). The canalicular porosity was estimated using a structural model that used five parameters either taken from the literature or measured from the analyzed osteons. The volume of the osteonal specimen, V_s (mm^3), the lacunar density, N_{Lac}/mm^3, and the inner and outer diameter of the osteon, r_i and r_o (μm), were derived from μCT and light microscopy images, while the average distance between two neighboring lacunae was evaluated using a parallelepiped periodic unit cell (PPUC) that surrounded a lacuna. The side dimension, L (μm), of the PPUC represents the center-to-center distance between two neighboring lacunae (Beno et al. 2006).

$$L=(V_s/N_{Lac})^{1/3}. \quad (9)$$

Based on Eq. (9), the average canaliculi length is

$$L_{Can}=L-2r_{Lac}. \quad (10)$$

where r_{Lac} is the average radius of lacunae in the radial direction, estimated to be approximately r_{Lac} = 2.5 μm (Beno et al. 2006). Finally, we use the diameter of the canaliculi reported in the literature as 259 ± 129 nm (You et al. 2004), and the number of canaliculi emanating from each lacuna as 62, based on the average of measurements reported in Beno et al. (2006) using the slicing method. The final formula for the canalicular porosity, $\phi_{Can,}$ is then

$$\varphi_{\mathrm{Can}}=\frac{62\,(129.5)^2\,\pi L_{\mathrm{Can}}}{V_{\mathrm{s}}}. \quad (11)$$

2.7 Tissue mineral density and elastic constants

In order to estimate the Young's elastic modulus of each osteon, the ρ_{HA} was obtained from μCT density-calibrated VOIs. Using the relationship between ρ_{HA} and E_r^m from Wagner et al. (2011)

$$\log_{10}E_r^m=-8.58+4.05\log_{10}\frac{400}{1+(504/\rho_{\mathrm{HA}})}, \quad (12)$$

where ρ_{HA} is the TMD obtained from the μCT, and the Young's modulus of the matrix material in the radial direction, E_r^m, was evaluated. The Young's modulus in the axial direction, E_z^m, was calculated based on the symmetry of the fourth-order transversely isotropic elasticity tensor,

$$\frac{E_r^m}{\nu_{rz}^m}=\frac{E_z^m}{\nu_{zr}^m}, \quad (13)$$

where the Poisson's ratios were $\nu_{zr}^m=0.312$ and $\nu_{rz}^m=0.255$ (Weinbaum et al. 1994).

2.8 Determination of the lacunar–canalicular permeability (K_{LC})

The lacunar–canalicular permeability was first determined from curve fitting of the analytical model (Benalla et al. 2012) against experimental data of $\tan[\bar{\delta}(\omega)]$ measured in the 1–100 Hz frequency range. The curve fitting was performed in MATLAB using a least-squares algorithm with a single free parameter, K_{LC}. Then, the lacunar–canalicular permeability was also obtained using Eq. (6), which represents the inverse solution for K_{LC} from the analytical poroelasticity model of the osteon under cyclic loading.

2.9 Statistical analysis

Descriptive statistics were obtained for the lacunar density (N_{Lac}/mm^3, #/mm^3), lacunar porosity (ϕ_{Lac}, %), canalicular porosity (ϕ_{Can}, %), lacunar–canalicular porosity (ϕ_{LC}, %), tissue mineral density (TMD, gHA/cm^3), Young's moduli in the radial, and axial directions (E_r^m and E_z^m, GPa). Repeated measures ANOVA and Tukey's multiple comparison tests were performed to identify differences in $\tan[\bar{\delta}(\omega)]$ and K_{rr} measured at different time points, as well as at different frequencies. Prior to performing statistical tests, normality was verified by the Kolmogorov–Smirnov test. All tests were performed using Prism statistics software (V.5.03, GraphPad, La Jolla, CA, USA) with a significance level of $p < 0.05$.

3 Results

3.1 Material properties and microstructure of isolated osteons

The mean ± SD values of the inner and outer radius for the sixty isolated human osteons were 41.5 ± 19.0 and 76.0 ± 32.5 μm, respectively. The volumetric lacunar density, N_{Lac}/mm^3, was found to be (36.85 ± 9.99) × 10^3 lacunae per mm^3. The average lacunar porosity, ϕ_{Lac}, estimated from μCT scans was 1.69 ± 0.50 %, and using the structural model described by Eq. (9), the average canalicular porosity, ϕ_{Can}, was found to be 2.79 ± 0.91 % (Table 1). These two porosities lead to an estimated lacunar–canalicular porosity, ϕ_{LC}, of 4.51 ± 2.01 %. The average tissue mineral density, TMD, or volumetric hydroxyapatite density, ρ_{HA}/cm^3, from μCT measurements was found to be 0.91 ± 0.06 g_{HA}/cm^3, which is used in Eqs. (12–13) to yield Young's moduli (Wagner et al. 2011) estimates of $E_r^m = 15.29 \pm 1.31$ GPa in the radial direction and $E_z^m = 18.72 \pm 1.61$ GPa in the axial direction.

3.2 Effect of osteon freshness on loss tangent

Changes in loss tangent measurements due to the lack of tissue freshness during the time elapsed between the isolation and loading of the sample were analyzed hourly and daily. No significant differences were found in $\tan[\bar{\delta}(\omega)]$ measurements within the first three hours after isolation of osteons (Fig. 1a). However, a small (~1%) but statistically significant ($p < 0.05$) change in $\tan[\bar{\delta}(\omega)]$ was found when measurements were taken 4 and 5 h after the samples were extracted. In addition, a clear, statistically significant decrease of $\tan[\bar{\delta}(\omega)]$ was found in measurements taken every 24 h, with $\tan[\bar{\delta}(\omega)]$ found to be almost 5 % lower at the fifth day of testing (Fig. 1b).

The hourly and daily changes in $\tan[\bar{\delta}(\omega)]$ (direct measurement from experiments) were also analyzed to determine whether such changes have a significant effect on K_{LC} (indirect estimates using analytical model). A change of 1 % in $\tan[\bar{\delta}(\omega)]$ observed in the osteon samples measured hourly resulted in a change in K_{LC} of less than 0.1 %, while the 5 % change in $\tan[\bar{\delta}(\omega)]$ from the osteon samples measured daily produced a change in K_{LC} of approximately 10 %. Therefore, to maintain tissue freshness, testing of osteons in the second experiment of this study was performed within 5 h of specimen cutting.

3.3 Intrinsic and dynamic permeability of human LCS

In this study, K_{LC} was obtained by two methods, namely the curve fitting of loss tangent data to the analytical model (Benalla et al. 2012) and by using the inverse solution of the poroelastic model (Eq. 6). In the first method, the experimental measurements of loss tangent at different loading frequencies were curve-fitted to the analytical model (Benalla et al. 2012), in which K_{LC} is the fitting parameter. This approach resulted in an average lacunar–canalicular permeability in the osteonal radial direction, K_{rr} = (2.34 ± 0.33) × $10^{-22} m^2$ (Fig. 2). Changes in loss tangent due to frequency were not statistically significant different at frequencies below 3 Hz, but differences were significant at 5 Hz and higher frequencies when compared to the loss tangent measured at 1Hz. Also, the standard deviation of the $\tan[\bar{\delta}(\omega)]$ decreased as the frequency increased. The K_{LC} measurements have an 11.4% coefficient of variation (CV = 100 × standard deviation/mean). In the second

method, using Eq. (6), the lacunar–canalicular permeability was found to vary between $(3.27\pm 0.45) \times 10^{-22}m^2$ and $(1.68\pm 0.11) \times 10^{-22}m^2$ when analyzed in the 1–100 Hz range, showing a linear decrease with respect to frequency at a rate of $-0.02 \times 10^{-22}m^2$/Hz (Fig. 3). The ordinate at the origin (zero frequency) represents the intrinsic K_{LC}, which was found to be $3.27 \times 10^{-22}m^2$. When compared to K_{LC} measured at 1 Hz, the lacunar–canalicular permeability showed no significant differences below 20 Hz, but changes were significant at 30 Hz and higher frequencies.

3.4 Loss tangent and K_{LC} as a function of the lacunar–canalicular porosity

The loss tangent versus lacunar–canalicular porosity (ϕ_{LC}) displays a linear behavior within the narrow range of porosity investigated (Fig. 4). The correlation between these two variables is $r^2 = 0.54$, and the equation of the linear fit model is $\tan[\bar{\delta}(\omega)] = 0.003\phi_{LC} + 0.027$. Similarly, the analysis of K_{LC} versus ϕ_{LC} exhibits a linear behavior, $K_{rr} = (0.27\phi_{LC} + 1.14) \times 10^{-22}m^2$, and a strong correlation coefficient, $r^2 = 0.86$ with $p < 0.05$ (Fig. 5).

4 Discussion

4.1 Material properties and microstructure of isolated osteons

There are not many measurements of the lacunar–canalicular porosity (ϕ_{LC}) reported to date; however, recent advances in 3D imaging have lead to measurement of several microarchitectural parameters of the lacunar–canalicular system, from where ϕ_{LC} can be estimated. The lacunar–canalicular microarchitecture includes the volumetric lacunar density, which represents the number of osteocyte lacuna measured per unit volume (#/mm^3), lacunar volume, inter-lacuna separation, canaliculi diameter, and number of primary and secondary (branching) canaliculi emanating from a lacuna (Table 1). The average lacunar porosity, ϕ_{Lac}, estimated from μCT scans in this study, 1.69 ± 0.50 %, using 2-μm resolution is in close agreement with the 1.3 % from Schneider et al. (2007) using 0.7-μm resolution in mice, the 1.5 % from Tommasini et al. (2012) using 0.75-μm resolution in rats, and the 1.5 ± 0.44 % lacunar porosity values reported by Palacio-Mancheno et al. (2013) using 1-μm resolution. Based on the structural model described by Eq. (9), the average canalicular porosity, ϕ_{Can}, was found to be 2.79 ± 0.91 %, which is in between the range of values, 0.7 and 14 %, reported by Schneider et al. (2011) using focused ion beam/scanning electron microscopy (FIB/SEM) and Sharma et al. (2012) using confocal laser scanning microscopy (CLSM), respectively. However, measurements of the canalicular porosity using CLSM seem to be overestimated due to partial volume effects. In our study, the addition of the lacunar and canalicular porosities lead to an estimated lacunar–canalicular porosity, ϕ_{LC}, of 4.51±2.01 %. The volumetric lacunar density (N_{Lac}/mm^3) of 36.85 ± 9.99(×10^3) lacunae per mm^3 measured in this study also falls within the range of values, 26 – 90 × 10^3 lacunae/mm^3, in other studies using synchrotron radiation-based micro-CT (SR-μCT) (Hannah et al. 2010; Tommasini et al. 2012; Carter et al. 2013), μCT (Palacio-Mancheno et al. 2013), and CLSM (Sharma et al. 2012). Interestingly, N_{Lac}/mm^3 seems to be significantly larger in rodents when compared to human data. Studies using CLSM and SR-μCT have found the average lacunar volume to fall in the range of 290–455 μm^3 (Sharma et al. 2012; McCreadie et al. 2004; Hannah et al. 2010; Carter et al. 2013). The inter-lacunar separation has been reported to vary between 22 and 40 μm in different species

in CLSM studies (Sharma et al. 2012; Sugawara et al. 2011, 2005), and using SR-μCT (Hannah et al. 2010). Canaliculi morphology measurements were reported in the early work of Marotti (1990), Marotti et al. (1995, 1985) and in several more recent studies. The average canaliculi diameter spans a range of 100–700 nm using electron microscopy (Sharma et al. 2012; Marotti 1990; You et al. 2004; Schneider et al. 2011), CLSM (Sharma et al. 2012; Sugawara et al. 2005), and atomic force microscopy (AFM) (Lin and Xu 2011). Canalicular diameter measurements are considered to be overestimated in studies using CLSM systems because of partial volume effects. Finally, an average of 41–115 primary canaliculi per lacuna was reported using CLSM measurements and estimates from light microscopy measurements (Sharma et al. 2012; Sugawara et al. 2005; Beno et al. 2006), as well as using FIB/SEM (Schneider et al. 2011). Secondary canaliculi, which may branch from the primary canaliculi directly connected to a lacuna, were found to be ~ 390 canaliculi per lacuna (Sharma et al. 2012), which is four times higher than the number of primary canaliculi reported in the same study (Table 1). The tissue mineral density from μCT measurements found in this study using 2.1-μm resolution, 0.91 ± 0.06 gHA/cm^3, is in general agreement with previous reports of TMD in human samples, 0.926 ± 0.035 and 1.047 ± 0.046gHA/cm^3, measured at 13.5 and 3.4-μm scanning resolution (Souzanchi et al. 2012), respectively. These TMD values from human tissue are slightly lower than TMD values reported in rodents, 1.13–1.36 gHA/cm^3 (Palacio-Mancheno et al. 2013; Matsumoto et al. 2006; Martin-Badosa et al. 2003; Windahl et al. 1999).

4.2 Effect of osteon freshness on loss tangent

A main objective of this study was to determine the K_{LC} of fresh human bone after excluding the effect of the vascular system permeability. The freshness of the specimen is one of the most important factors for improving the accuracy in determining K_{LC}. Bone tissue loses some of its freshness with time and storage conditions, despite precautions that can be taken. Keeping the bone specimens hydrated with physiological solution and performing the experiment immediately after the specimen isolation are critical for acquiring ex vivo measurements that are as close as possible to the in vivo condition. Plots of $\tan[\bar{\delta}(\omega)]$ obtained from loaded osteons versus time show a decline of less than 1 % for a time duration of five hours and a decline of 5 % for a period of five days. The 1 % decrease of $\tan[\bar{\delta}(\omega)]$ does not significantly affect the final result of K_{LC}, while the 5 % decrease reduces K_{LC} by 10 %. In this study, we have made every effort to preserve the freshness of the osteons by storing them immersed in PBS and loading them within five hours after isolation.

4.3 Intrinsic permeability of human LCS

The estimates of lacunar–canalicular permeability in Table 2 exhibit a broad range of values, from 10^{-17} to 10^{-25} m^2, with a noticeable 2–3 orders of magnitude difference between the average permeability value obtained from theoretical approaches (10^{-17} to 10^{-20} m^2) and experimental/theoretical approaches (10^{-22} to 10^{-25} m^2). In this study, the values of K_{LC} obtained by both curve fitting and inverse poroelastic model, 2.34×10^{-22}m^2 and 3.27×10^{-22}m^2, respectively, are much closer to the predicted values of K_{LC} by several theoretical analyses. Overall, these K_{LC} values lie in the middle range of values reported from theoretical and experimental studies (Table 2). Data also exhibit a small coefficient of

variability (14.1 %) when compared to previous reports in the literature (Table 2), possibly due to the individual measurement of ϕ_{LC} and tissue elastic modulus for each osteon.

There may be several reasons for the wide range of K_{LC} in previous studies (Cardoso et al. 2013) The first reason is related to the specimen size. A limitation associated with data from experimental studies that have used millimeter size or larger bone samples is that the resulting measurements correspond to the combination of the VS and LCS permeability due to the intermingling of the vascular and lacunar–canalicular pores. Such permeability measurements are thus dominated by the vascular pores, which are much larger than the lacunar–canalicular pores. In order to measure the K_{LC} only, the VS should not be included in the sample to be tested. The second reason is related to the material properties of the specimen. In most previous work, the material properties of the bone were adopted from the literature and generalized to all the samples. The adopted values may be close to the real ones; however, certain parameters, such as the ϕ_{LC}, may have a significant effect on the analytical model, which causes a significant variation in the determination of the K_{LC}. The sensitivity of the model parameters (Benalla et al. 2012) indicated that the ϕ_{LC} and Young's modulus were among the most influential parameters on the measurement of K_{LC}. Therefore, instead of adopting a single value of ϕ_{LC} and Young's modulus of the tissue matrix material from the literature, these parameters were determined separately for each osteon specimen. The average Young's moduli of the matrix material in the radial (15.29 ± 1.31 GPa) and axial (18.72 ± 1.61 GPa) directions as well as the ϕ_{LC} (4.51 ± 2.01 %) were found to be in close agreement with values reported by others (Goulet et al. 2009; Orias et al. 2009; Cardoso et al. 2013). The individual determination of these parameters increased the accuracy in determining K_{LC}. Third, this large variability in the lacunar–canalicular permeability is likely influenced by theoretical assumptions and experimental errors associated with the measurement of a very small quantity. Performing direct measurements on samples with very small permeability and very small size (i.e., samples 100–250 μm in diameter and 0.5 mm in height) is highly sensitive to measurement errors. Fourth, the freshness of the tissue seems very important to obtain appropriate values of permeability. When the tissue is no longer fresh, or has been treated (i.e., dehydrated, resin infiltrated, and embedded), its properties change, and the lacunar–canalicular pores may be not be as open as in their natural state and result in smaller permeability estimates. Fifth, several theoretical estimates analyze the lacunar–canalicular system considering open pores at both ends of the LCS. However, the knowledge of boundary conditions of the analytical model used to estimate the lacunar–canalicular permeability is generally imprecise. Sixth, there exist hydroelectrochemical effects associated with fluid flow in canaliculi (Lemaire et al. 2012) that could significantly influence the permeability of the LCS, which are not fully elucidated to date.

4.4 Dynamic permeability of human LCS

The second goal of this study was to investigate the dependence of K_{LC} on loading frequency. It was found that as the frequency increases from 1 to 100 Hz, K_{LC} decreases linearly at a rate of -0.02×10^{-22} m^2/Hz, from $3.25 \times 10^{-22} m^2$ to $1.82 \times 10^{-22} m^2$ (Fig. 3). The inverse relationship between K_{LC} and frequency is considered to be mainly related to the decrease in the loss modulus and the increase in the storage modulus in the matrix

material (Figs. 3 and 4 in Benalla et al. (2012)). Because the relaxation time associated with the LCS is around 4.9 ms (Zhang et al. 1998), which corresponds to ~ 200 Hz, it is expected that the decreasing rate of K_{LC} will increase after 200 Hz because the LCS pore pressure will not have enough time to relax entirely. The incomplete relaxation of the LCS will cause the interstitial fluid to lower its velocity between all the lacunae and through the canaliculi, which will amplify the decreasing rate of K_{LC} at loading frequencies higher than 200 Hz. It was noted that the coefficients of variation of $\tan[\bar{\delta}(\omega)]$ and K_{LC} are larger at low frequency and keep decreasing as the frequency increases (Figs. 2 and 3). This observation is explained by the fact that at high frequencies, the mechanical behavior of the osteon becomes purely elastic (Figs. 3 and 4 in Benalla et al. 2012).

4.5 Effect of ϕ_{LC} on $\tan[\bar{\delta}(\omega)]$ and K_{LC}

The sensitivity study in Benalla et al. (2012) showed that ϕ_{LC} is one of the most influential parameters of the model inputs. Therefore, the variability of K_{LC} and $\tan[\bar{\delta}(\omega)]$ versus ϕ_{LC} was also studied. Strong relationships were found between $\tan[\bar{\delta}(\omega)]$ and ϕ_{LC} (Fig. 4) as well as between K_{LC} and ϕ_{LC} (Fig. 5) for the sixty loaded osteons. The high correlation, $r^2 = 0.86$ ($p < 0.05$), of the permeability with respect to porosity (Fig. 5) shows that there is a strong linear relation-ship between the two parameters and suggests that the variability of K_{LC} depends mainly on ϕ_{LC}. Thus, the equation of the linear fit model, $K_{rr} = (0.27\phi_{LCS} + 1.14) \times 10^{-22}\text{m}^2$, represents an empirical formula to predict the K_{LC} from ϕ_{LC} measurements. However, the correlation between loss tangent versus porosity, $r^2 = 0.54$ ($p < 0.05$), illustrates that $\tan[\bar{\delta}(\omega)]$ is not dependent on the ϕ_{LC} alone and that other parameters such as the elastic constants and inner and outer osteonal radius are also involved.

4.6 Study limitations

There are several limitations in this study. First, the idealization of the osteon and the Haversian canal as pure cylinders is not fully correct. The shape of the osteon and the Haversian canal is not purely circular, and their radii may slightly change from bottom to top. However, the small height of the osteon sections, 500 μm, minimizes the inaccuracy of this assumption. Second, in the evaluation of the lacunar–canalicular porosity, the canaliculi are considered to be straight tubes relating the lacunae with each other and with the Haversian canal. In reality, some of these canaliculi, especially the ones emanating from the apices of the lacunae, radiate along the vertical axis of the lacunae before they bend horizontally following the radial direction Marotti (1996). Nonetheless, only few canaliculi take that bent shape, which reduces their effect. The third limitation is related to the assumption of considering the outer boundary of the osteon to be impermeable. However, interstitial fluid flow across the cement line, if it exists, should be negligible compared to fluid flow at the surface of the Haversian canal. Finally, the ϕ_{Lac} was estimated using μCT scans with a 2.1-μm resolution. A more accurate estimate of ϕ_{Lac} could be obtained with a nanoCT system.

Acknowledgments

This work was supported by NSF (PHY-0848491, CMMI-1333560, MRI-0723027, and 1229449), NIH/NIA (AG34198), PSC-CUNY Research Award Program of the City University of New York and by a fellowship from the CUNY Graduate Center.

References

Anderson EJ, Kreuzer SM, Small O, Tate MLK. Pairing computational and scaled physical models to determine permeability as a measure of cellular communication in micro- and nano-scale peri-cellular spaces. Microfluid Nanofluid. 2008; 4(3):193–204.10.1007/s10404-007-0156-5

Benalla M, Cardoso L, Cowin SC. Analytical basis for the determination of the lacunar-canalicular permeability of bone using cyclic loading. Biomech Model Mechanobiol. 2012; 11(6):767–780.10.1007/s10237-011-0350-y [PubMed: 21959747]

Beno T, Yoon YJ, Cowin SC, Fritton SP. Estimation of bone permeability using accurate microstructural measurements. J Biomech. 2006; 39(13):2378–2387.10.1016/j.jbiomech.2005.08.005 [PubMed: 16176815]

Cardoso L, Fritton SP, Gailani G, Benalla M, Cowin SC. Advances in assessment of bone porosity, permeability and interstitial fluid flow. J Biomech. 2013; 46(2):253–265.10.1016/j.jbiomech.2012.10.025 [PubMed: 23174418]

Carter Y, Thomas CD, Clement JG, Peele AG, Hannah K, Cooper DM. Variation in osteocyte lacunar morphology and density in the human femur-a synchrotron radiation micro-CT study. Bone. 2013; 52(1):126–132.10.1016/j.bone.2012.09.010 [PubMed: 22995461]

Cowin SC, Gailani G, Benalla M. Hierarchical poroelasticity: movement of interstitial fluid between porosity levels in bones. Philos Transact A Math Phys Eng Sci. 2009; 367(1902):3401–3444.10.1098/rsta2009.0099

Dillaman RM. Movement of ferritin in the 2-day-old chick femur. Anat Rec. 1984; 209(4):445–453.10.1002/ar.1092090404 [PubMed: 6476415]

Fritton SP, Weinbaum S. Fluid and solute transport in bone: flow-induced mechanotransduction. Annu Rev Fluid Mech. 2009; 41:347–374.10.1146/annurev.fluid.010908.165136 [PubMed: 20072666]

Gailani G, Benalla M, Mahamud R, Cowin SC, Cardoso L. Experimental determination of the permeability in the lacunar-canalicular porosity of bone. J Biomech Eng. 2009; 131(10):101007.10.1115/1.3200908 [PubMed: 19831477]

Gailani G, Cowin SC. The unconfined compression of a porous annular cylindrical disk. J Mech Mater. 2008; 40(6):507–523.

Gailani G, Cowin SC. Ramp loading in Russian doll poroelasticity. J Mech Phys Solids. 2011; 53:103–120.

Galli M, Oyen ML. Fast identification of poroelastic parameters from indentation test. Comput Model Eng Sci. 2009; 48:241–270.

Gardinier JD, Townend CW, Jen KP, Wu Q, Duncan RL, Wang L. In situ permeability measurement of the mammalian lacunarcanalicular system. Bone. 2010; 46(4):1075–1081.10.1016/j.bone.2010.01.371 [PubMed: 20080221]

Goulet GC, Coombe D, Martinuzzi RJ, Zernicke RF. Poroelastic evaluation of fluid movement through the lacunocanalicular system. Ann Biomed Eng. 2009; 37(7):1390–1402.10.1007/s10439-009-9706-1 [PubMed: 19415492]

Gururaja S, Kim HJ, Swan CC, Brand RA, Lakes RS. Modeling deformation-induced fluid flow in cortical bone's canalicularlacunar system. Ann Biomed Eng. 2005; 33(1):7–25. [PubMed: 15709702]

Hannah KM, Thomas CDL, Clement JG, De Carlo F, Peele AG. Bimodal distribution of osteocyte lacunar size in the human femoral cortex as revealed by micro-CT. Bone. 2010; 47(5):866–871.10.1016/j.bone.2010.07.025 [PubMed: 20691298]

Johnson MW. Behavior of fluid in stressed bone and cellular stimulation. Calcif Tissue Int. 1984; 36(Suppl 1):S72–76. [PubMed: 6430527]

Kameo Y, Adachi T, Sato N, Hojo M. Estimation of bone permeability considering the morphology of lacunocanalicular porosity. J Mech Behav Biomed Mater. 2010; 3(3):240–248.10.1016/j.jmbbm.2009.10.005 [PubMed: 20142108]

Lemaire T, Lemonnier S, Naili S. On the paradoxical determinations of the lacunocanalicular permeability of bone. Biomech Model Mechanobiol. 201210.1007/s10237-011-0363-6

Lemaire T, Naili S, Remond A. Study of the influence of fibrous pericellular matrix in the cortical interstitial fluid movement with hydroelectrochemical effects. J Biomech Eng. 2008; 130(1): 011001.10.1115/1.2838025 [PubMed: 18298177]

Li GP, Bronk JT, An KN, Kelly PJ. Permeability of cortical bone of canine tibiae. Microvasc Res. 1987; 34(3):302–310. [PubMed: 2448591]

Lin Y, Xu S. AFM analysis of the lacunarcanalicular network in demineralized compact bone. J Microsc. 2011; 241(3):291–302.10.1111/j.1365-2818.2010.03431.x [PubMed: 21118225]

Malachanne E, Dureisseix D, Canadas P, Jourdan F. Experimental and numerical identification of cortical bone permeability. J Biomech. 2008; 41(3):721–725.10.1016/j.jbiomech.2007.09.028 [PubMed: 18023447]

Marotti, G. The original contributions of the scanning electron microscope to the knowledge of bone structure. In: Bonucci, E.; Motta, PM., editors. Ultrastructure of skeletal tissues. Boston: Kluwer Academic; 1990. p. 19-39.

Marotti G. The structure of bone tissues and the cellular control of their deposition. Ital J Anat Embryol. 1996; 101(4):25–79. [PubMed: 9203871]

Marotti G, Ferretti M, Remaggi F, Palumbo C. Quantitative evaluation on osteocyte canalicular density in human secondary osteons. Bone. 1995; 16(1):125–128. [PubMed: 7742070]

Marotti G, Muglia MA, Zaffe D. A SEM study of osteocyte orientation in alternately structured osteons. Bone. 1985; 6(5):331–334. [PubMed: 4096864]

Martin-Badosa E, Amblard D, Nuzzo S, Elmoutaouakkil A, Vico L, Peyrin F. Excised bone structures in mice: imaging at three-dimensional synchrotron radiation micro CT. Radiology. 2003; 229(3): 921–928.10.1148/radiol.2293020558 [PubMed: 14657323]

Matsumoto T, Yoshino M, Asano T, Uesugi K, Todoh M, Tanaka M. Monochromatic synchrotron radiation muCT reveals disuse-mediated canal network rarefaction in cortical bone of growing rat tibiae. J Appl Physiol. 2006; 100(1):274–280.10.1152/japplphysiol.00495.2005 [PubMed: 16141381]

McCreadie BR, Hollister SJ, Schaffler MB, Goldstein SA. Osteocyte lacuna size and shape in women with and without osteoporotic fracture. J Biomech. 2004; 37(4):563–572.10.1016/S0021-9290(03)00287-2 [PubMed: 14996569]

Neuman WF, Toribara TY, Mulryan BJ. The surface chemistry of bone 7. The hydration shell. J Am Chem Soc. 1953; 75(17):4239–4242.

Orias AAE, Deuerling JM, Landrigan MD, Renaud JE, Roeder RK. Anatomic variation in the elastic anisotropy of cortical bone tissue in the human femur. J Mech Behav Biomed. 2009; 2(3):255–263.10.1016/j.jmbbm.2008.08.005

Oyen ML. Poroelastic nanoindentation responses of hydrated bone. J Mater Res. 2008; 23(5):1307–1314.10.1557/Jmr2008.0156

Palacio-Mancheno PE, Larriera AI, Doty SB, Cardoso L, Fritton SP. 3D assessment of cortical bone porosity and tissue mineral density using high-resolution micro-CT: effects of resolution and threshold method. J Bone Miner Res. 201310.1002/jbmr.2012

Remaggi F, Cane V, Palumbo C, Ferreti M. Histomorphometric study on the osteocyte lacunocanalicular network in animals of different species. I. Woven-fibered and parallel fibered bones. Ital J Anat Embryol. 1998; 103:145–155. [PubMed: 9882957]

Rouhana SW, Johnson MW, Chakkalakal DA, Harper RA. Permeability of the osteocyte lacunocanalicular compact bone. Joint ASME ASCE Conf Biomech Symp AMD. 1981; 43:169–172.

Schneider P, Meier M, Wepf R, Muller R. Serial FIB/SEM imaging for quantitative 3D assessment of the osteocyte lacunocanalicular network. Bone. 2011; 49(2):304–311.10.1016/j.bone.2011.04.005 [PubMed: 21514408]

Schneider P, Stauber M, Voide R, Stampanoni M, Donahue LR, Muller R. Ultrastructural properties in cortical bone vary greatly in two inbred strains of mice as assessed by synchrotron light based micro- and Nano-CT. J Bone Miner Res. 2007; 22(10):1557–1570.10.1359/Jbmr.070703 [PubMed: 17605631]

Sharma D, Ciani C, Marin PAR, Levy JD, Doty SB, Fritton SP. Alterations in the osteocyte lacunarcanalicular microenvironment due to estrogen deficiency. Bone. 2012; 51(3):488–497.10.1016/j.bone.2012.05.014 [PubMed: 22634177]

Smit TH, Huyghe JM, Cowin SC. Estimation of the poroelastic parameters of cortical bone. J Biomech. 2002; 35(6):829–835. [PubMed: 12021003]

Souzanchi MF, Palacio-Mancheno P, Borisov YA, Cardoso L, Cowin SC. Microarchitecture and bone quality in the human calcaneus: local variations of fabric anisotropy. J Bone Miner Res. 2012; 27(12):2562–2572.10.1002/jbmr.1710 [PubMed: 22807141]

Sugawara Y, Ando R, Kamioka H, Ishihara Y, Honjo T, Kawanabe N, Kurosaka H, Takano-Yamamoto T, Yamashiro T. The three-dimensional morphometry and cell-cell communication of the osteocyte network in chick and mouse embryonic calvaria. Calcif Tissue Int. 2011; 88(5):416–424.10.1007/s00223-011-9471-7 [PubMed: 21340572]

Sugawara Y, Kamioka H, Honjo T, Tezuka K, Takano-Yamamoto T. Three-dimensional reconstruction of chick calvarial osteocytes and their cell processes using confocal microscopy. Bone. 2005; 36(5):877–883.10.1016/j.bone.2004.10.008 [PubMed: 15820146]

Swan CC, Lakes RS, Brand RA, Stewart KJ. Micromechanically based poroelastic modeling of fluid flow in Haversian bone. J Biomech Eng. 2003; 125(1):25–37. [PubMed: 12661194]

Tommasini SM, Trinward A, Acerbo AS, De Carlo F, Miller LM, Judex S. Changes in intracortical microporosities induced by pharmaceutical treatment of osteoporosis as detected by high resolution micro-CT. Bone. 2012; 50(3):596–604.10.1016/j.bone.2011.12.012 [PubMed: 22226688]

Wagner DW, Lindsey DP, Beaupre GS. Deriving tissue density and elastic modulus from microCT bone scans. Bone. 2011; 49(5):931–938. [PubMed: 21820094]

Wang L, Fritton SP, Cowin SC, Weinbaum S. Fluid pressure relaxation depends upon osteonal microstructure: modeling an oscillatory bending experiment. J Biomech. 1999; 32(7):663–672. [PubMed: 10400353]

Wehrli FW, Fernandez-Seara MA. Nuclear magnetic resonance studies of bone water. Ann Biomed Eng. 2005; 33(1):79–86. [PubMed: 15709708]

Weinbaum S, Cowin SC, Zeng Y. A model for the excitation of osteocytes by mechanical loading-induced bone fluid shear stresses. J Biomech. 1994; 27(3):339–360. [PubMed: 8051194]

Wen D, Androjna C, Vasanji A, Belovich J, Midura RJ. Lipids and collagen matrix restrict the hydraulic permeability within the porous compartment of adult cortical bone. Ann Biomed Eng. 2010; 38(3):558–569.10.1007/s10439-009-9858-z [PubMed: 19967451]

Windahl SH, Vidal O, Andersson G, Gustafsson JA, Ohlsson C. Increased cortical bone mineral content but unchanged trabecular bone mineral density in female ERbeta(−/−) mice. J Clin Invest. 1999; 104(7):895–901.10.1172/JCI6730 [PubMed: 10510330]

You L, Cowin SC, Schaffler MB, Weinbaum S. A model for strain amplification in the actin cytoskeleton of osteocytes due to fluid drag on pericellular matrix. J Biomech. 2001; 34(11):1375–1386. [PubMed: 11672712]

You LD, Weinbaum S, Cowin SC, Schaffler MB. Ultrastructure of the osteocyte process and its pericellular matrix. Anat Rec A Discov Mol Cell Evol Biol. 2004; 278(2):505–513.10.1002/ar.a.20050 [PubMed: 15164337]

Zhang D, Weinbaum S, Cowin SC. Estimates of the peak pressures in bone pore water. J Biomech Eng. 1998; 120(6):697–703. [PubMed: 10412451]

Zhou X, Novotny JE, Wang L. Modeling fluorescence recovery after photobleaching in loaded bone: potential applications in measuring fluid and solute transport in the osteocytic lacunarcanalicular system. Ann Biomed Eng. 2008; 36(12):1961–1977.10.1007/s10439-008-9566-0 [PubMed: 18810639]

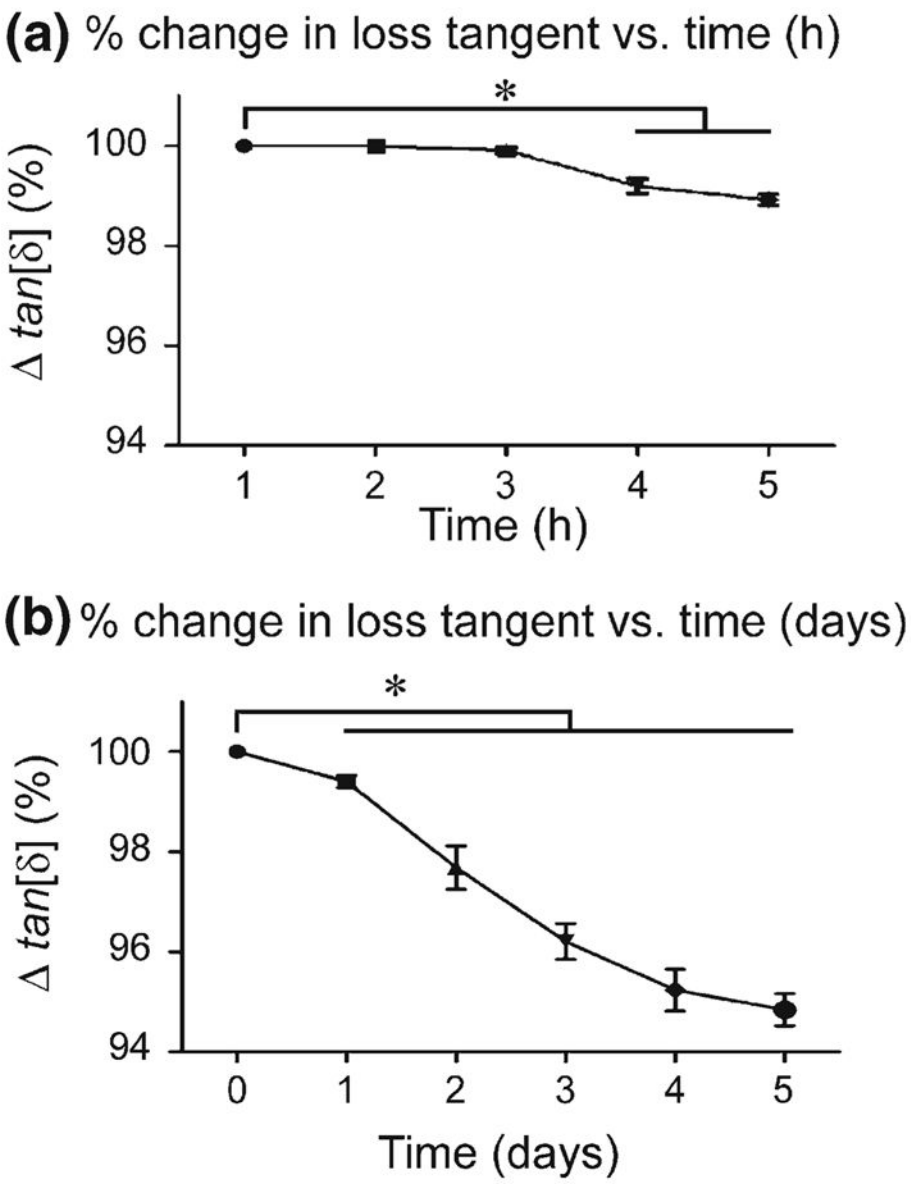

Fig. 1.

a The loss tangent (mean ± SD) versus time for a period of 5 h. **b** The loss tangent (mean ± SD) versus time for a duration of 5 days (* $p<0.05$, nine loaded osteons in each analysis)

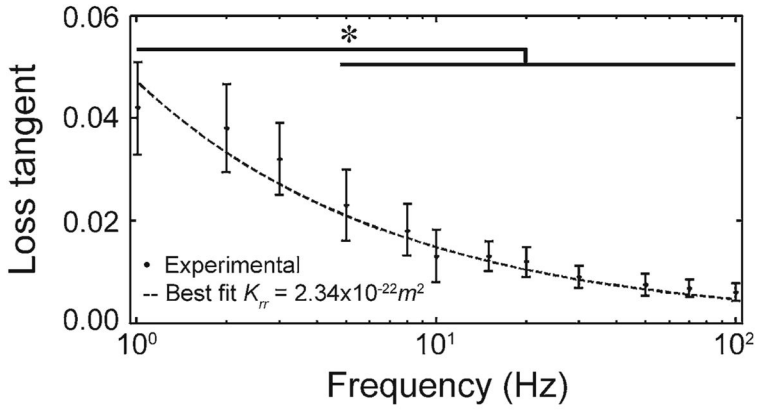

Fig. 2.

Curve fitting of the analytical model and experimental data of the loss tangent to evaluate the average lacunar–canalicular permeability, $K_{rr} = (2.34 \pm 0.33) \times 10^{-22}\text{m}^2$($^* p < 0.05$, sixty loaded osteons)

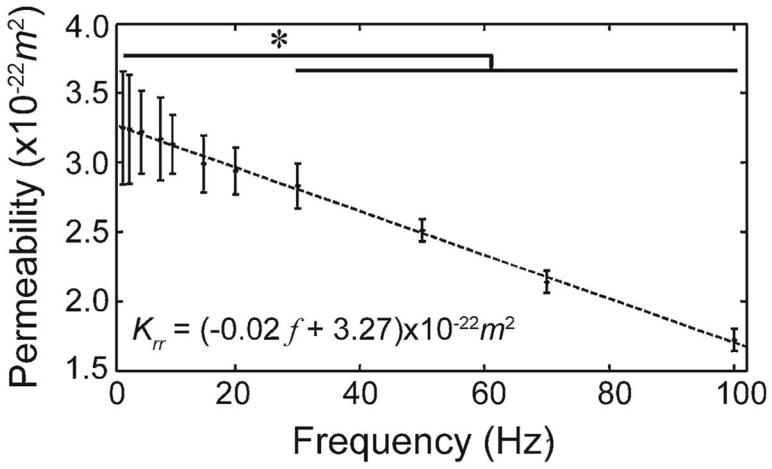

Fig. 3.

Lacunar–canalicular permeability versus frequency, $K_{rr} = (3.27 - 0.02\,f) \times 10^{-22}\mathrm{m}^2$(* $p <$ 0.05, sixty loaded osteons) from inverse poroelastic model of K_{rr}

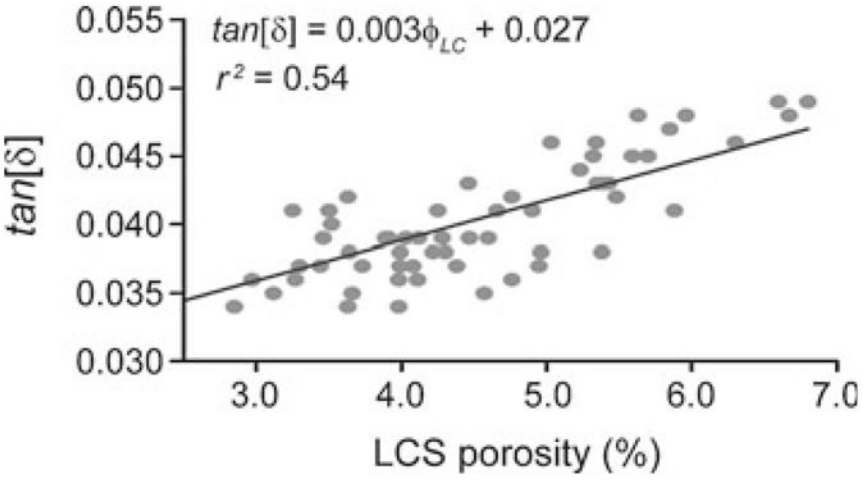

Fig. 4.

Loss tangent, tan [$\delta(\omega = 2\pi)$], measured at 1 Hz cyclic loading of isolated human osteons versus lacunar–canalicular porosity, ϕ_{LC} (sixty loaded osteons)

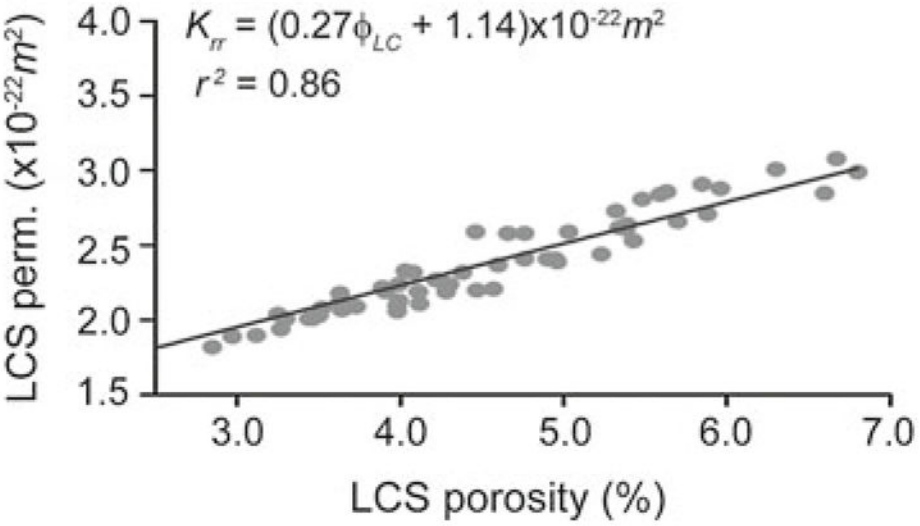

Fig. 5.

Lacunar–canalicular permeability in the radial direction of isolated human osteons, K_{rr}, versus lacunar–canalicular porosity, ϕ_{LC} (sixty loaded osteons)

Table 1

Measurements and estimates of micro/nanoarchitecture of the lacunar–canalicular network (updated from Cardoso et al. 2013)

Reference	Method	Tissue	Lacunar porosity (%)
Schneider et al. (2007)	SR-μ CT	Mouse (B6) femoral mid-diaphysis	1.3
Tommasini et al. (2012)	SR-μ CT	Rat femoral diaphysis	1.5
Palacio-Mancheno et al. (2013)	μ CT	Rat tibial cortical metaphysis	1.5 ± 0.44
Present study	μ CT	Human femoral diaphysis	1.69 ± 0.50
Reference	Method	Tissue	Canalicular porosity (%)
Schneider et al. (2011)	FIB/SEM	Mouse (B6) femoral mid-diaphysis	0.70
Sharma et al. (2012)	CLSM	Rat tibial cortical metaphysis	14 (overestimated due to partial volume effects)
Present study	μ CT	Human femoral diaphysis	2.79 ± 0.91
Reference	Method	Tissue	Lacuna per unit volume (#/mm^3)
Hannah et al. (2010)	SR-μ CT	Human femur	40–90 (×10^3)
Tommasini et al. (2012)	SR-μ CT	Rat femoral diaphysis	56.5 (×10^3)
Sharma et al. (2012)	CLSM	Rat tibial cortical metaphysis	67.3 ± 14.0 (×10^3)
Carter et al. (2013)	SR-μ CT	Human femur	26–37 (×10^3)
Palacio-Mancheno et al. (2013)	μ CT	Rat tibial cortical metaphysis	68.8 ± 13.2 (×10^3)
Present study	μ CT	Human femoral diaphysis	36.85 ± 9.99 (×10^3)
Reference	Method	Tissue	Lacunar volume (μ m^3)
McCreadie et al. (2004)	CLSM	Human hip	455 ± 200
Hannah et al. (2010)	SR-μ CT	Human femur	290 ± 107
Sharma et al. (2012)	CLSM	Rat tibial cortical metaphysis	352 ± 30
Carter et al. (2013)	SR-μ CT	Human femur	~400
Reference	Method	Tissue	Inter-lacuna separation (μ m)
Sugawara et al. (2005)	CLSM	Chick calvaria, E16 days old	24.1 ± 2.8
Hannah et al. (2010)	SR-μ CT	Human femur	21.9 ± 6.3
Sugawara et al. (2011)	CLSM	Chick calvaria, E16 days old	23.5 ± 6.1
		Mouse calvaria (B6), E17 days old	39.6 ± 11.6
Sharma et al. (2012)	CLSM	Rat tibial cortical metaphysis	24.8 ± 1.7
Reference	Method	Tissue	Canaliculi diameter (nm)
Marotti (1990)	SEM	Human tibia	150–550
You et al. (2004)	TEM	Mouse female	259 ± 129
Sugawara et al. (2005)	CLSM	Chick calvaria, E16 days old	<500
Lin and Xu (2011)	AFM	Bovine tibia, transverse direction	426 ± 118
		Bovine tibia, radial direction	459 ± 144

Reference	**Method**	**Tissue**	**Lacunar porosity (%)**
		Bovine tibia, longitudinal direction	419 ± 113
Schneider et al. (2011)	FIB/SEM	Mouse (B6) femoral mid-diaphysis	95
Sharma et al. (2012)	CLSM	Rat tibia, cortical metaphysis trab. remnants	520 ± 42
		Rat tibia, cortical metaphysis lamellar region	553 ± 33
		Rat tibia, cancellous metaphysis	483 ± 24
	SEM	Rat tibia, cancellous metaphysis	335 ± 32
	TEM	Rat tibia, cancellous metaphysis	228 ± 11
Reference	Method	Tissue	# canaliculi per lacuna
Sugawara et al. (2005)	CLSM	Chick calvaria, E16 days old	52.7 ± 5.7
Beno et al. (2006)	Estimated from (Remaggi et al. 1998) light microscopy data	Chick	54
		Rabbit	60
		Bovine	85
		Horse	115
		Dog	81
		Human	41
Schneider et al. (2011)	FIB/SEM	Mouse (B6) femoral mid-diaphysis	78
Sugawara et al. (2011)	CLSM	Chick calvaria, E16 days old	52.7 ± 6.4
		Mouse calvaria (B6), E17 days old	49.7 ± 9.7
Sharma et al. (2012)	CLSM	Rat tibia, primary canaliculi	83.9 ± 14
		Rat tibia, secondary canaliculi	387 ± 34

μCT micro-computed tomography, *CLSM* confocal laser scanning microscopy, *SR-μCT* synchrotron radiation-based micro-CT, *TEM* transmission electron microscopy, *AFM* atomic force microscopy, *FIB/SEM* focused ion beam/scanning electron microscopy

Table 2

Measurements and estimates of intrinsic permeability in the vascular and lacunar–canalicular systems (updated from Cardoso et al. 2013)

Reference	Method (theoretical estimate)	Tissue	VS permeability (m^2)
Johnson (1984)	Theoretical study	–	2.5×10^{-14}
Dillaman (1984)	Theoretical study	Rat	1×10^{-13} to 1×10^{-11}
Zhang et al. (1998)	Theoretical study	–	1×10^{-15} to 1×10^{-13}
Swan et al. (2003)	Theoretical study	–	1.25×10^{-13} to 3×10^{-12}
Reference	Method (experimental measurement)	Tissue	VS permeability (m^2)
Rouhana et al. (1981)	Perfusion	Bovine	3×10^{-13}
Li et al. (1987)	Perfusion	Canine	5×10^{-17} to 1×10^{-15}
Malachanne et al. (2008)	Compression and FEA	Bovine, ox femurs	1.1×10^{-13}
Wen et al. (2010)	Perfusion	Canine	4×10^{-17}
Reference	Method (theoretical estimate)	Tissue	LCS permeability (m^2)
Weinbaum et al. (1994)	Ultrastructural model	–	1.0×10^{-22} to 1.0×10^{-19}
Zhang et al. (1998)	Theoretical, adapted from Weinbaum et al. (1994)	–	1.5×10^{-20}
Wang et al. (1999)	Theoretical, adapted from Weinbaum et al. (1994)	–	1.0×10^{-21} to 1.3×10^{-19}
Smit et al. (2002)	Finite element analysis	–	2.2×10^{-22}
Gururaja et al. (2005)	Theoretical, adapted from Weinbaum et al. (1994)	–	7.5×10^{-20}
Beno et al. (2006)	Adapted from Weinbaum et al. (1994)	Chick, rabbit, bovine, horse, dog, human (data from Remaggi et al. 1998)	1.0×10^{-22} to 1.0×10^{-19}
Lemaire et al. (2008)	Glycocalyx fiber permeability, adapted from Weinbaum et al. (1994)	–	5.9×10^{-18} to 2.0×10^{-17}
Anderson et al. (2008)	Perfusion on scaled-up models and predictive virtual and stochastic computational models	Scaled-up, rapid prototyped models of human femoral neck	2.7×10^{-18} to 8.7×10^{-18}
Cowin et al. (2009)	Poroelasticity theory	–	1.5×10^{-20}
Goulet et al. (2009)	Carman–Kozeny permeability model	–	1.0×10^{-18} to 1.0×10^{-20}
Kameo et al. (2010)	Morphology of LCP using CLSM	Swine tibia	3.3×10^{-19} to 1.3×10^{-18}
Lemaire et al. (2012)	FEM, Carman–Kozeny permeability model	–	1.0×10^{-19} to 1.0×10^{-18}
Reference	Method (experimental measurement)	Tissue	LCS permeability (m^2)

Reference	Method (theoretical estimate)	Tissue	VS permeability (m^2)
Oyen (2008)	Nanoindentation poroelasticity	Human	4.1×10^{-24}
Galli and Oyen (2009)	Nanoindentation poroelasticity	Human	6.5×10^{-23}
Zhou et al. (2008)	FRAP poroelasticity	Mice	1.0×10^{-21}
Gailani et al. (2009)	Stress relaxation single osteons poroelasticity	Bovine	$5.0 \times 10^{-25} – 8.0 \times 10^{-24}$
Gardinier et al. (2010)	Step loading in vivo poroelasticity	Canine	2.8×10^{-23}
Present study	Harmonic loading of isolated osteons	Human femoral diaphysis	$2.34 \times 10^{-22} \pm 0.33 \times 10^{-22}$